

# PCCP

Accepted Manuscript



This is an *Accepted Manuscript*, which has been through the Royal Society of Chemistry peer review process and has been accepted for publication.

*Accepted Manuscripts* are published online shortly after acceptance, before technical editing, formatting and proof reading. Using this free service, authors can make their results available to the community, in citable form, before we publish the edited article. We will replace this *Accepted Manuscript* with the edited and formatted *Advance Article* as soon as it is available.

You can find more information about *Accepted Manuscripts* in the [Information for Authors](#).

Please note that technical editing may introduce minor changes to the text and/or graphics, which may alter content. The journal's standard [Terms & Conditions](#) and the [Ethical guidelines](#) still apply. In no event shall the Royal Society of Chemistry be held responsible for any errors or omissions in this *Accepted Manuscript* or any consequences arising from the use of any information it contains.

## Electronic properties of mixed valence hydrated europium chloride thin film

Cite this: DOI: 10.1039/x0xx00000x

M. G. Silly<sup>a</sup>, F. Charra<sup>b</sup>, F. Lux<sup>c</sup>, G. Lemerrier<sup>d</sup>, F. Sirotti<sup>a</sup>

Received 00th January 2012,  
Accepted 00th January 2012

DOI: 10.1039/x0xx00000x

www.rsc.org/

We investigate the electronic properties of a model mixed-valence hydrated chloride europium salt by means of high resolution photoemission spectroscopy (HRPES) and resonant photoemission spectroscopy (RESPES) at the Eu 3d→4f and 4d→4f transitions. From the HRPES spectra, we have determined that the two europium oxidation states are homogeneously distributed into the bulk and that the hydrated salt film is exempt of surface mixed valence transition. From the RESPES spectra, the well separated resonant contributions characteristic of divalent and trivalent europium species (4f<sup>6</sup> and 4f<sup>7</sup> final states, respectively) are accurately extracted and quantitatively determined from the resonant features measured at the two edges. The partial absorption yield spectra, obtained by integrating the photoemission intensity in the valence-band region, can be well reproduced by atomic multiplet calculation at the M<sub>4,5</sub> (3d-4f) absorption edge and by an asymmetric Fano-like shape profile at the N<sub>4,5</sub> (4d-4f) absorption edge. The *ratio* of Eu<sup>2+</sup> and Eu<sup>3+</sup> species measured at the two absorption edges match with the composition of the mixed valence europium salt as determined chemically. We have demonstrated that the observed spectroscopic features of mixed valence salt are attributed to mixed-valence ground state rather than surface valence transition. HRPES and RESPES spectra provide reference spectra for the study of europium salts and their derivatives.

### 1 Introduction

Due to their optical properties, rare-earth ions know high interest for applications in photoactive organometallic compounds such as light-emitting devices (OLEDs, phosphors, ...), chemical and biological sensors, wavelength photo converters for photovoltaic applications.<sup>1</sup> More recently rare-earth ions in dielectric crystals have also shown high potential in quantum information processing as optical quantum memories or as quantum repeaters in quantum communication devices.<sup>2-6</sup> Nevertheless, despite the 4f core shielding by the surrounding filled 5s and 5p shells, luminescent<sup>7</sup> and electronic<sup>6</sup> properties of Eu ions suffer from their sensitivity to the chemical environment such as counter ion, water and solvent, at the origin of inhomogeneous broadening on optical transitions<sup>6</sup> limiting the bandwidth and the efficiency of quantum memory based on electromagnetically induced transparency.<sup>8-10</sup> Moreover, Eu luminescent emission strongly depends on 4f states: while Eu<sup>3+</sup> presents a pure atomic-line-like red luminescence, Eu<sup>2+</sup> exhibits a strong UV broad band luminescence.<sup>11</sup>

Recently a stable phase in UHV of a hydrated EuCl<sub>2,85</sub> salt has been evidenced.<sup>12</sup> In general mixed-valence compounds present high interest in electronic application as fast ion conductors but also mixed ionic-electronic conductors.<sup>13</sup> They notably find application as solid electrolytes or electrodes in energy storage domains as substituent to liquid electrolytes. The specific conducting properties are governed by defects and they depend directly on the amount, arrangement and localization of the different ions in the bulk. It has been demonstrated that the conductivity of europium oxide significantly varies with its stoichiometry<sup>14</sup> and can be tuned to match that of silicon.<sup>15,16</sup> But the amount and the location of the oxygen vacancies at the origin of the doping are still difficult to assess.<sup>17</sup>

An accurate determination in the composition of the salt combined with a better understanding of the spatial distribution into the ionic solid of the different oxidation states of the europium is susceptible to provide insights on the expected conductivity of the salt. It has been shown that in trivalent Rare-Earth (RE) compounds, surface valence transitions to the divalent state accompany the change in coordination at the surface which favors the lower-valence state of the RE ions.<sup>18,19</sup>

This process manifests itself as a surface core level shift in photoemission spectroscopy experiments.<sup>20,21</sup> Although trivalent Eu contribution measured in photoemission was for a while explained by shake-up excitations in insulating RE compounds,<sup>22</sup> this explanation has been finally refuted in favor of surface valence transition.<sup>21</sup> The origin of divalent europium can be unambiguously identified by measuring the core level spectra at different photon energy and taking into account the different electron escape depth  $\lambda$  depending on the photoelectron kinetic energy.<sup>23,24</sup> If the  $\text{Eu}^{2+}$  species are located at the surface, the electrical conduction will come from the domain boundary, whereas if they are homogeneously distributed, the charges will lead to bulk conduction. The deviation from stoichiometry of pure hydrated  $\text{EuCl}_3$  salt induces structural disorder and electronic compensation leading to the creation of electronic defects, here, lower oxidation states ( $\text{Eu}^{2+}$ ) at the origin of electrical conductivity. An excess in metallic ions leads to n doped semiconductors. Whereas many studies have been conducted about metal oxides and alloys, few ones have focused on europium salts. The signature of the electronic structure and the potential interactions with ligands in europium salt is missing. A better understanding of these interactions, which often limit the device performances, is needed in view of the development of applications.

Independently to high resolution core level photoemission spectroscopy (HRPES), Near-edge X-ray Absorption Fine Structure (NEXAFS) and resonant photoemission spectroscopy (RESPES) techniques according to their high chemical sensitivity have been used, mainly to study the composition of mixed valence compounds. Due to the large 4f photoemission enhancement observed at the 3d, 4d  $\rightarrow$  4f resonance, absorption and resonant photoemission spectroscopies represent powerful tools to study valence changes of rare-earth ions in dilute systems and at surfaces.<sup>25</sup> These techniques have been successfully employed to determine oxidation states in various mixed valence compounds including europium based metallic oxides,<sup>26</sup> europium intermetallic compounds,<sup>27,28</sup> and magnetic compounds,<sup>29,30</sup> nevertheless surface effects such as surface valence changes in intermetallic compounds underline the extreme care needed to interpret the measured signals.<sup>31</sup> Actually, in solid state, the complexity and the increased number of different recombination processes contributing to features observed in resonant photoemission experiments can lead to supplementary information about e.g. charge transfer processes.<sup>32,33</sup> Usually, NEXAFS experiment needs a spectroscopic reference to properly assign the electronic properties and chemical composition of a material.<sup>12,31,34</sup> Here it is shown that the use of the combination of HRPES, NEXAFS and RESPES overcomes this limitation and provides a powerful method to determine both the composition as well as the distribution of the various oxides at the surface.<sup>29</sup>

In this paper, we report a detailed study on high-resolution 4d photoelectron spectra and resonant soft X-rays 3d $\rightarrow$ 4f and 4d $\rightarrow$ 4f excitations of hydrated mixed valence europium salt. We provide a reference of the electronic structure of the  $\text{EuCl}_{2.85}$  salt composed of a mixture of  $\text{Eu}^{2+}$  and  $\text{Eu}^{3+}$  ions. From the different spectroscopic techniques, we extract the signature of each hydrated europium chloride salt valence. By comparison with theoretical models describing the X-ray absorption spectra of pure valence species, we have determined the contribution of each species, we have quantified them and we have confirmed the homogeneous repartition of the oxides

in the salt. We have shown the accuracy and the complementarity of HRPES and RESPES to characterize the electronic properties of complex mixed valence compounds such as europium based ionic solid.

## 2 Experimental setup

Hydrated europium chloride thin films were formed on gold substrate by depositing commercial  $\text{EuCl}_3 \cdot 6\text{H}_2\text{O}$  salt (Acros) with purity of 99.9%. Samples were prepared by dissolving  $\text{EuCl}_3 \cdot 6\text{H}_2\text{O}$  salt in dry ethanol. The solution was then deposited on the gold substrate, and solvent was evaporated at 50°C under  $\text{N}_2$  gas flux. Gold substrates were 100 nm thick layers of gold epitaxially grown on mica. Before use, they were  $\text{H}_2$  flame annealed at about 450°C in air in order to obtain clean Au(111)- $22\sqrt{3}$  reconstructed terraces.

A recent study<sup>12</sup> based on a combination of chemical dosing, core level photoemission spectroscopy, X-ray absorption, and photoluminescence showed that europium salt prepared following this procedure and placed in UHV environment presents a homogeneous assembly of hydrated  $\text{EuCl}_2$  and  $\text{EuCl}_3$  species. Chemical dosing by ionic chromatography leads to a  $\text{EuCl}_{2.85 \pm 0.05}$  composition in good agreement, within measurement accuracy, with electronic properties exhibiting contribution of 15%  $\langle \text{Eu}^{2+} \rangle$  and 80%  $\langle \text{Eu}^{3+} \rangle$  species.

The Eu 4d HRPES, X-ray absorption spectroscopy (XAS) and RESPES experiments at Eu 3d $\rightarrow$ 4f and 4d $\rightarrow$ 4f absorption edges were performed at the French Synchrotron Facility Soleil at the soft X-ray TEMPO beamline<sup>35</sup>. The XAS was performed recording the drain sample current as a function of photon energy and normalized to gold mesh signal (60% transmission). The HRPES and RESPES experiments were performed using a hemispherical electron analyser Scienta 2002 equipped with a fast delay line detector.<sup>36</sup> The total resolving power of the experiments (beamline and electron energy analyser resolving power was better than 5000). Measurements were performed at a pressure lower than  $3.10^{-10}$  mbars. To analyze europium ion absorption spectra measured at 3d $\rightarrow$ 4f and 4d $\rightarrow$ 4f transitions, atomic multiplet calculations were performed using the CTM4XAS 5.23 program<sup>37</sup> based on Cowan atomic calculation codes.<sup>38</sup>

The inelastic electron mean free paths for the hydrated  $\text{EuCl}_3 \cdot 6\text{H}_2\text{O}$  salt were calculated using the QUASES-IMFP-TPP2M software based on the Tanuma Powell and Penn algorithm (TPP2M).<sup>39</sup> A bulk density of 4.89 g/cm<sup>3</sup> and a molecular weight of 366.414 u are used according to the literature.<sup>40</sup>

Resonant photoemission experiments were performed by scanning the photon energy of an impinging soft-X ray beam across the threshold energy needed to excite an electronic transition from a core level to allowed empty states. In the case of Europium we have studied 3d $\rightarrow$ 4f and 4d $\rightarrow$ 4f electronic excitations located around 1130 eV and 150 eV, respectively. The process is schematized in Figure 1. In the X-ray absorption process a core-electron is photo-excited into a resonant bound state [Fig.1.1]. The system can then relax *via* Auger and

fluorescence transitions involving all external electronic states. Two types of Auger processes are possible in the relaxation process. In the participator-type Auger transition the photoexcited electron itself is involved in Auger emission process [Fig. 1] and disperses with a constant binding energy [Fig. 1.2], while spectator Auger and normal Auger disperse with constant kinetic energy when the photon energy is scanned through the absorption edge [Fig. 1.3].

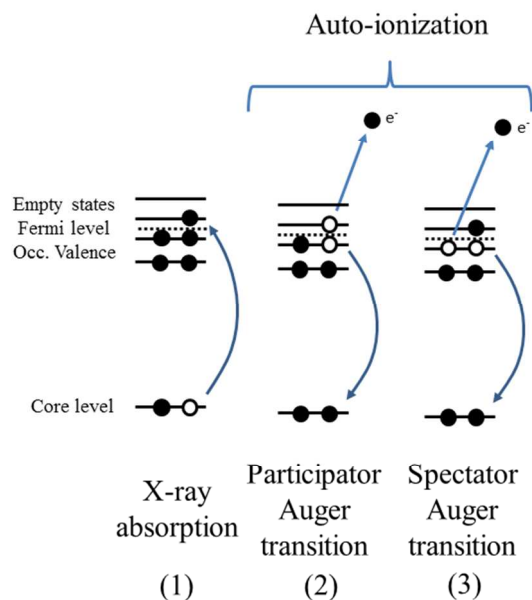


Fig. 1: Schematics of electronic orbital diagram describing the resonant photoemission excitation and de-excitation processes. (1) Resonant X-ray absorption, exciting photon energy corresponds to a transition from an occupied core level to a valence band empty state. (2) and (3) de-excitation processes accompanied by emission of electrons referred to as participator (2) and spectator (3) Auger transitions, respectively.

We measured valence-band resonant photoemission spectra by analyzing in a binding energy range of about 20 eV below  $E_F$  and observed the de-excitation processes in which valence electrons are directly involved. The outcome of the experiment is a three dimensional map where the photoemission intensity is presented as a function of impinging photon energy and binding energy as deduced from photo-electron kinetic energy. Further details on the techniques can be found elsewhere.<sup>30, 41</sup>

During the resonant photoemission experiment, the Total Electron Yield (TEY) emitted can be measured as a function of the photon energy by detecting the overall drain current. The X-ray absorption spectrum can be directly superimposed onto the resonant photoemission map.  $\text{Eu}^{2+}$  and  $\text{Eu}^{3+}$  absorption spectra were simulated using calculations based on the atomic multiplet theory for divalent and trivalent europium at  $3d \rightarrow 4f$  absorption edge using the CTM4XAS 5.23 program.<sup>37</sup> The discrete energy states are broadened with a Gaussian and a Lorentzian shape to take into account enlargement of discrete energy states due to instrumental resolution and core-hole lifetime, respectively.

### 3 Results and discussion

#### 3.1 Core level photoemission

In figure 2, we report the Eu 4d core level photoemission spectra, presenting the final state of the hydrated mixed valence compound salt, measured at two photon energies.

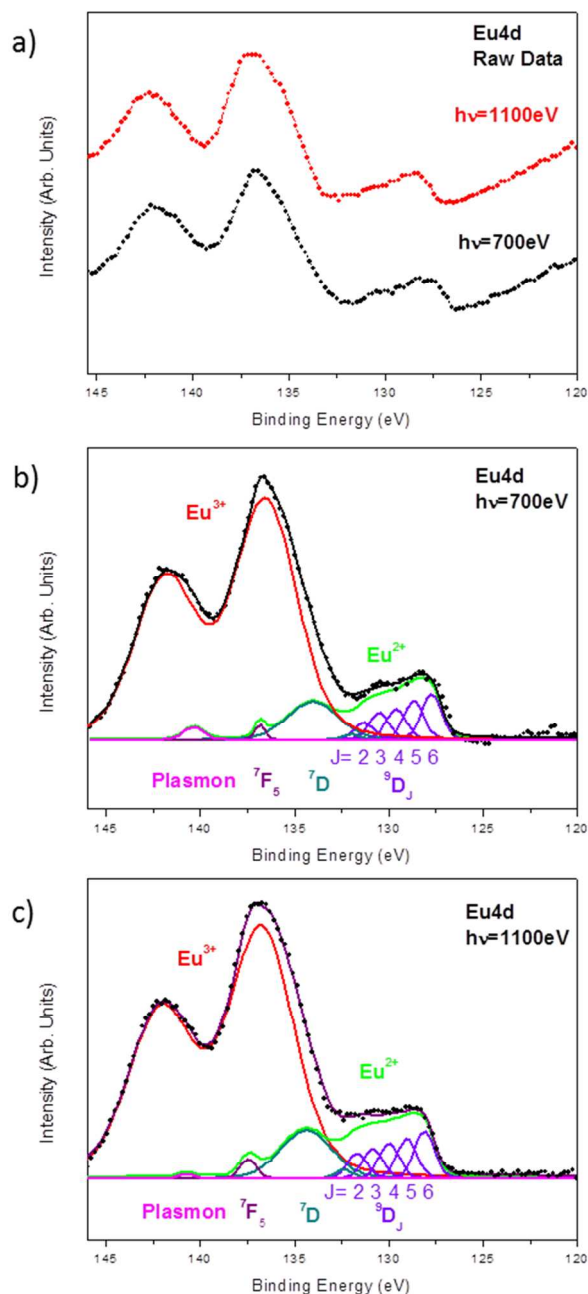


Fig. 2: a) High resolution Eu 4d photoelectron spectra of the hydrated  $\text{EuCl}_{2.85}$  mixed valence salt measured at 700 eV and 1100 eV to perform a depth profile analysis. The results of curve fitting for the spectra measured at 700 eV (b) and 1100 eV (c) are presented. The divalent feature exhibits complex shape caused by 4d-4f interactions, the signal is deconvoluted according to Ref.<sup>42</sup>

By comparing the 4d core level spectra measured for two different photon energies, figure 2a, a depth profile analysis is performed to extract the distribution of the divalent europium in the thin film. Here we show that the shape of the 4d core level spectra does not exhibit noticeable modification for photon energies of 700 eV and 1100 eV corresponding to 570 eV and 970 eV in kinetic energy, respectively. The two kinetic energies correspond to an electron inelastic mean free path ( $\lambda$ ) of 13.14 Å and 19.38 Å, respectively. At normal emission, the probability of electron escape depth  $\phi(z)$  follows a Beer-Lambert law:

$$\phi(z) \propto \exp(-z/\lambda)$$

Integrating the equation with respect to the depth ( $z$ ), it appears that 95% of the photoemission signal is originated in the first  $3\lambda$  in thickness. The measured core level spectra are very sensitive to the signal originated from the surface. To quantitatively determine the variation of the  $\text{Eu}^{2+}$  and  $\text{Eu}^{3+}$  amount as a function of photon energy, we have performed a fine decomposition of the core level spectra. In figure 2b and c, the Eu 4d core level spectra which are measured at 700 eV and 1100 eV in photon energy, respectively, are deconvoluted using Voigt functions. Components located at lower binding energy correspond to  $\text{Eu}^{3+}$  states, a standard Voigt doublet taking into accounts for the spin orbit splitting of 5.3 eV and a ratio of 2:3 for the  $4d_{3/2}$  and  $4d_{5/2}$  states, respectively. To match with the experimental data a Gaussian broadening of 1.5 eV is used. The remaining signal located at higher kinetic energy related to the  $\text{Eu}^{2+}$  states exhibits a more complex shape due to multiplet interactions. The  $\text{Eu}^{2+}$  4d core level spectra exhibit the characteristic multiplet structure induced by strong interaction between 4d hole and unfilled 4f shell, as the two electron shells have the same principal quantum number. The  $\text{Eu}^{2+}$  4d core level is deconvoluted according to experimental and theoretical work on atomic europium.<sup>42</sup> The coupling between d-hole and the ground state configuration of Eu leads mainly to  ${}^7D_J$  ( $J = 1$  to 5) states and  ${}^9D_J$  ( $J = 2$  to 6) states, but two other contributions attributed to plasmon and  ${}^7F_5$  state are also noticeable at higher binding energy. Compared to the energy position found in atomic europium,<sup>42</sup> the binding energy positions in the salt are shifted by 8.2 eV in lower binding energy. Indeed, the values in gas phase have to be pondered by the work function of the solid and the cohesive energy varying according to the europium environment and the chemical bonding.<sup>43</sup> The binding energy positions we find for Eu salt are close to that found in europium based semiconductors,<sup>29,44</sup> europium intermetallic<sup>20</sup> and insulating compounds.<sup>21,22</sup> For the deconvolution of the  ${}^9D$  states, we use the natural line width of 0.2 eV,<sup>42</sup> to match the data, we determine a Gaussian broadening of 0.7 eV higher than the instrumental resolution. The FWHM of the  ${}^9D$  transitions gives a direct insight of the disorder, inhomogeneity and defects in the sample and of the electronic interactions with surrounding ligands in the crystal; as both of them result in a broadening of the different components. Compared to the literature, the FWHM appears to be larger than that one observed in atomic europium<sup>42</sup> or in well define crystals as  $\text{Eu}_{1-x}\text{Gd}_x\text{Te}$  semiconductor<sup>29</sup> but is comparable to that one measured for insulating Eu compounds presenting mixed valence transition.<sup>21,22</sup> Mainly two phenomena contribute to the observed broadening, the high sensitivity of the europium ion to the molecular environment and notably the interaction with surrounding ligands ( $\text{Cl}^-$ ,  $\text{H}_2\text{O}$ ) enlarging the optical transition as observed in THz experiments<sup>6</sup> and the coexistence of  $\text{Eu}^{3+}$  and  $\text{Eu}^{2+}$  oxidation states in the salt introducing  $\text{Cl}^-$  vacancies into the crystal

assembly. In comparison, we have seen that the  $\text{Eu}^{3+}$  4d component presents a Gaussian broadening of 1.5 eV higher than the broadening for  $\text{Eu}^{2+}$   ${}^9D$  states. As a ionic crystal is governed by Coulomb interaction between the ions, the  $\text{Eu}^{3+}$  oxide also present a high sensitivity to the chemical environment and is affected by the crystal defect induced by the  $\text{Eu}^{2+}$ .

From the contribution coming from the divalent and trivalent europium, we calculate the  $\text{Eu}^{2+}:\text{Eu}^{3+}$  ratio for the two photon energies (700 eV and 1100 eV). In spite of the peak fitting uncertainty due to a close imbrication of the divalent and trivalent europium signals, we find, in both cases, a  $\text{Eu}^{2+}:\text{Eu}^{3+}$  ratio of 2:8 corresponding to 20% of divalent europium. As the  $\text{Eu}^{2+}:\text{Eu}^{3+}$  ratio remains constant as a function of the probing photon energy, we can conclude that no surface processes are responsible for the observed  $\text{Eu}^{2+}$  contribution. This result argues in favor of a homogeneous repartition of the divalent europium in the salt. The determined  $\text{Eu}^{2+}:\text{Eu}^{3+}$  ratio, although slightly higher than the expected ratio of 15% of divalent europium determined by chemical dosing, remains within the error bar.<sup>12</sup>

### 3.1 Resonant photoemission signal

The resonant photoemission signal of the europium ion is measured at the 4d and 3d absorption edges where the spectroscopic signals coming from the two oxidation states are well separated.<sup>26-33</sup>

The results obtained at the Eu 3d $\rightarrow$ 4f transition ( $M_{4,5}$  absorption edge) are reported in Fig. 3. In figure 3a, the black curve represents the XAS spectrum measured in total electron yield in the photon energy range 1118 -1178 eV. Two main contributions located at 1131 and 1158.9 eV are visible and correspond to Eu 3d $_{5/2}\rightarrow$ 4f and 3d $_{3/2}\rightarrow$ 4f transitions, respectively. The observed features are consistent with a signal dominated by  $\text{Eu}^{3+}$  species<sup>45,46</sup> but the slight shoulder located at 1128.8eV (indicated by black stick in the top panel in Fig. 3a) denotes a noticeable contribution of  $\text{Eu}^{2+}$ . The detailed shape is in good agreement with an atomic multiplet structure of a mixture of  $\text{Eu}^{2+}/\text{Eu}^{3+}$  species.<sup>27</sup>

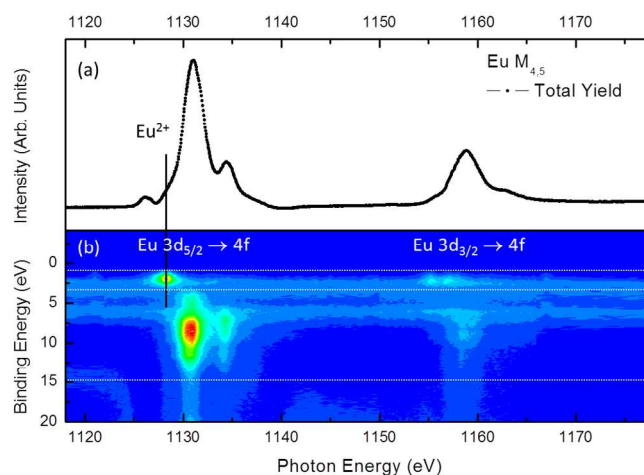


Fig. 3: (a) Near band edge X-ray absorption spectrum for mixed valence  $\text{EuCl}_{2.85}$  salt deposited on Gold(111) reconstructed surface measured in the photon energy range of the  $\text{Eu}3d\text{-}4f$  ( $M_{4,5}$  absorption edge) in TEY mode. (b) Resonant

photoemission map for the photon energy (1118–1178 eV) corresponding to the  $3d \rightarrow 4f$  absorption edges. Right part corresponds to the  $3d_{3/2} \rightarrow 4f$  transitions. Left part is related to  $3d_{5/2} \rightarrow 4f$  transitions, dash lines delimit area of localized resonant states.

The origin of the structures corresponding to the different oxidation states identified in the X-ray absorption spectrum can be better disentangled by observing the resonant photoelectron spectroscopy map measured in the binding energy range between the Fermi level and 25 eV as reported in Fig 3b. The photoemission intensity is presented in a pseudo-color scale as a function of the photon energy (x axis) and of the electron binding energy (y axis). Due to the large photoionization cross section at  $3d \rightarrow 4f$  transition, resonant photoemission is very sensitive to the europium species. The resonant signals coming from the various oxidation states exhibit sharp and well separated structures. The oxidation states present in the sample can be unambiguously ascribed and accurately quantified. Looking at the resonant intensity we can discern the contributions from two Resonant Auger decay channels localized at two well defined energy regions within the binding energy scale. When gradually increasing the photon energy, in the Eu  $3d_{3/2} \rightarrow 4f$  transitions, we first identify a sharp single resonance located at 2.2 eV in binding energy. In the literature, this feature is commonly attributed to  $\text{Eu}^{2+}$  states.<sup>27,47</sup> It is followed by a broader resonant peak located between 3 and 12 eV with a maximum close to 9 eV. This second structure is interpreted in terms of  $\text{Eu}^{3+}$  resonances.<sup>27</sup> The same behavior is observed at the Eu  $3d_{5/2} \rightarrow 4f$  transitions at about 1160 eV where a resonant state located at 2.25 eV and a broad resonance centered at 7 eV are also ascribed to  $\text{Eu}^{2+}$  and  $\text{Eu}^{3+}$  states, respectively.

The resonant components shift linearly with the photon energy and are in good agreement with participator-type Auger transition models. The observed resonant de-excitation pathways involving discrete  $3d \rightarrow 4f$  transitions, they lead to the emission of 4f valence electrons of well-defined binding energy. From the intensity map one can extract resonant absorption line profiles by isolating each resonant state in its own well defined integration domain of binding energies (partial yield). The integrated profiles of the resonant photoemission lines located at binding energy of 2.26 eV and 7 eV (Fig. 3) are reported in the top panel figure 4a. In order to unambiguously ascribe resonant features to different europium species we compare the partial yield resonant profile to the results of atomic multiplet calculations. The calculated  $\text{Eu}3d \rightarrow 4f$  XAS spectra of  $\text{Eu}^{2+}$  and  $\text{Eu}^{3+}$  species are reported in the central panel figure 4b. They well reproduce the partial yield spectra reported in top panel figure 4a. Discrete energy states whose broadening leads to absorption spectrum are presented in the bottom panel of figure 4c. The best match with the experimental data was obtained with a Gaussian half-width half-maximum of 0.6 eV representing the experimental broadening and a Lorentzian half-width half-maximum of 0.2 eV in good agreement with core hole natural width used in theoretical study.<sup>45</sup> The main features present in each valence of europium are well reproduced: the main peaks at 1128.3 eV and the double structure at 1131 and 1134.4 eV can be ascribed to the divalent and trivalent ions, respectively. The energy position of  $\text{Eu}^{2+}$  contribution fits with the shoulder at 1128.8 eV.

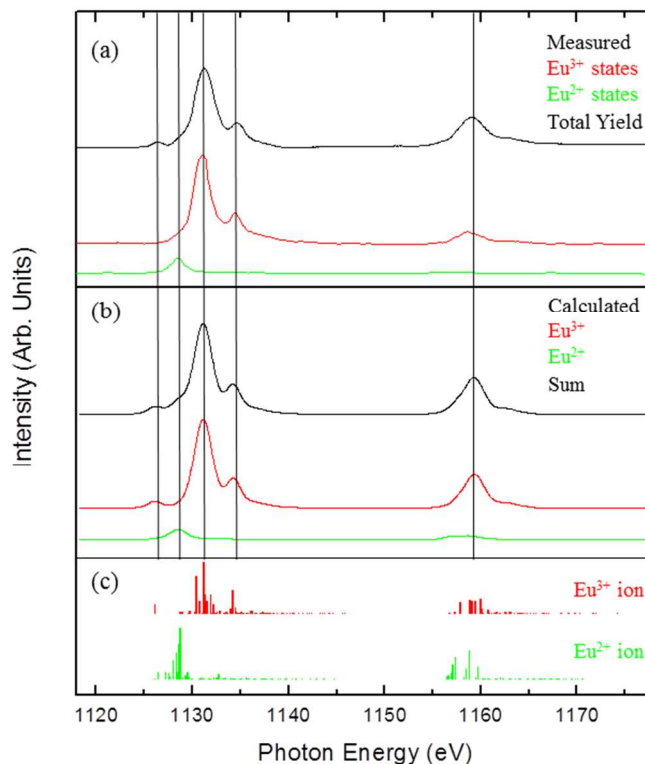
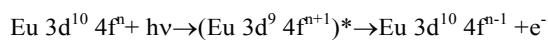


Fig. 4: (a)  $M_{4,5}$  absorption edges (black line) measured in TEY. Red and green lines are obtained by integrating the resonant valence band photoemission intensity around the two main structures situated at 2.26 eV and 7 eV binding energies, respectively. (b) Europium  $M_{4,5}$  absorption spectra calculated using an atomic multiplet model with the CTM4XAS 5.23 program. The  $\text{Eu}^{3+}$  and  $\text{Eu}^{2+}$  valences are presented in red and green whereas we present in black the sum of the two with a relative weight of 15 and 85% respectively. (c) Sticks corresponding to discrete energy states of intra-atomic multiplet excitation of  $\text{Eu}^{2+}$  and  $\text{Eu}^{3+}$  ions.

Nevertheless, some differences in the partial yield spectra must be underlined. The small peak at 1126.2 eV photon energy in the trivalent Eu ion is not observed in the partial yield spectra but is present in the Total Electron Yield spectrum of Fig. 4. This means that the decay process following this absorption is not accompanied with the emission of electron coming from the valence band region. The relative intensity of the  $M_4$  and  $M_5$  absorption edge measured in TEY is not the same observed in the MVV partial yield spectra. The  $M_4$  structure measured in partial yield must be multiplied by a factor 3.1 to reach the same spectral intensity obtained in Total Electron Yield mode. This is due to a  $M_4M_5V$  Coster Kronig decay in the Eu  $M_4$  excited state of the same order of the one observed on transition metals.<sup>48</sup> The good match of the  $\text{Eu}^{2+}$  and  $\text{Eu}^{3+}$  calculated multiplet spectral structure to integrated resonant photoemission lines located at binding energy of 2.26 eV and 7 eV permits to unambiguously assign the two measured resonant features to the two different oxidation states. We can conclude that resonant photoemission processes at  $M_{4,5}$  absorption edges are explained in sole terms of discrete intra-atomic multiplet transitions broadened by core-hole lifetime and instrumental resolution.

The resonant signals can consequently be explained in terms of two steps excitation/des-excitation processes verifying the following transitions:



where “\*” denotes an excited state,  $n$  corresponds to the number of electrons filling the 4f level and is equal to  $n=6$  or  $7$  for  $\text{Eu}^{2+}$  or  $\text{Eu}^{3+}$  states, respectively. The final states are hence equivalent to that which would result from a direct photoemission process of electrons out of the 4f levels. Due to the large photoionization cross section at  $3d \rightarrow 4f$  transition, photoemission process from 4f states is highly favored, which explains the high sensitivity to Europium oxidation states in relation with 4f filling. The Eu 4f feature for the divalent europium appearing at 1128.8 eV and made of a single contribution centered at 2.2 eV in binding energy is very sensitive to the chemical environment of the europium ion and will be discussed later with the resonant  $\text{Eu}^{2+}$  4f signal measured at the  $4d \rightarrow 4f$  transition. Finally, as the resonant electronic contribution coming from the  $\text{Eu}^{3+}$  and  $\text{Eu}^{2+}$  species are well separated, we determine the  $\text{Eu}^{2+}:\text{Eu}^{3+}$  ratio from the integrated profiles of the resonant photoemission lines located at binding energy of 2.26 eV and 7 eV. We calculate a relative weight of 15% in  $\text{Eu}^{2+}$  and 85% in  $\text{Eu}^{3+}$  for an inelastic electron mean free path of 21.76 Å.

RESPES spectra measured at the Eu  $4d \rightarrow 4f$  transition ( $N_{4,5}$  absorption edge) are reported in Figure 5. The X-ray absorption spectrum measured in Total Electron Yield at the  $4d \rightarrow 4f$  transition is reported in the top panel. Compared to the  $3d \rightarrow 4f$  edge, the  $4d \rightarrow 4f$  XAS spectrum presents a singular broaden and asymmetric shape. The  $4d \rightarrow 4f$  transition is known to exhibit a response characteristic of Fano-like shape component. This effect is related to localized excited states in the continuum. Clearly visible at the  $4d \rightarrow 4f$  transition edge, this behavior does not exist for  $3d \rightarrow 4f$  transitions presenting, as demonstrated above, a sharp resonant structure of atomic multiplet transitions with only Gaussian and Lorentzian broadenings of their discrete energy states.

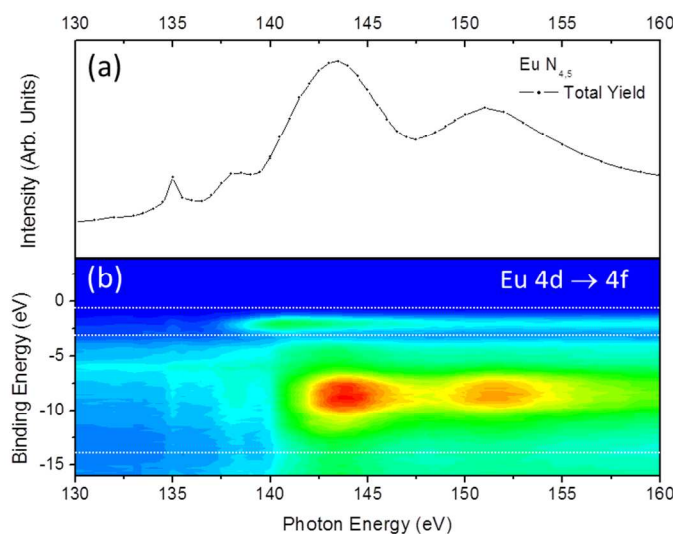
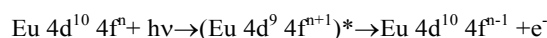


Fig. 5: (a) TEY X-ray absorption spectrum of  $\text{EuCl}_3$  salt measured at  $4d \rightarrow 4f$  absorption edge. (b) Resonant photoemission map in the binding energy range 0-16 eV measured while scanning the photon energy range 130-160 eV across the  $\text{Eu } N_{4,5}$   $4d \rightarrow 4f$  absorption edge. Dash lines delimit area of localized resonant states.

As shown in a previous study,<sup>31</sup> the signal coming from the  $\text{Eu}^{2+}$  and  $\text{Eu}^{3+}$  states are too close in energy at the  $4d \rightarrow 4f$  absorption edge to be clearly disentangle without any salt reference with  $\text{Eu}^{2+}/\text{Eu}^{3+}$  ratio. Indeed the single total yield NEXAFS spectrum is not sufficient to determine the ratio of  $\text{Eu}^{2+}$  and  $\text{Eu}^{3+}$  species. In order to quantify the amount of the two europium oxidation states, RESPES spectrum has been measured.

The map reproducing the photoemission intensity measured when photon energy crosses the  $4d \rightarrow 4f$  absorption edges is reported in the bottom panel of figure 5. The intensity distribution is very similar to the one observed at the  $M_5$  absorption edge. As seen in  $3d \rightarrow 4f$  transition, two main resonant features are visible. The first one located at a binding energy of 2 eV is normally induced by  $\text{Eu}^{2+}$  states and the second located around 7.5 eV is commonly associated with  $\text{Eu}^{3+}$  states.<sup>29, 31-33</sup> Similarly to  $3d \rightarrow 4f$  transitions, the resonant signals at  $4d \rightarrow 4f$  is described by a two-step excitation/de-excitation process according to the following equation:



With “\*” designating an excited state,  $n$  corresponding to the number of electrons filling the 4f level equal respectively to  $n=6$  or  $7$  for  $\text{Eu}^{2+}$  or  $\text{Eu}^{3+}$  states. The observed final states are equivalent to those which would result from a direct photoemission process of electrons coming from 4f levels. Photoemission processes occurring from 4f states exhibit a high sensitivity to Europium oxidation states due to large photoionization cross section at the  $4d \rightarrow 4f$  transition. At the  $\text{Eu}^{2+}$   $4d \rightarrow 4f$  on resonance, having a closer attention to the  $\text{Eu}^{2+}$  resonant feature, we notice that, as seen in the  $\text{Eu}^{2+}$   $3d \rightarrow 4f$  on-resonance, the  $\text{Eu}^{2+}$  4f contribution is composed of a single component located at relatively high energy compared to the literature.<sup>20,27,47</sup> In mixed valence transition compounds, Eu 4f feature is made of two components corresponding to bulk and surface contributions located respectively at lower and higher binding energy and usually separated by less than 1 eV.<sup>20,27,47</sup> The high binding energy of the  $\text{Eu}^{2+}$  4f component, that we measure, better fits with surface state made of incomplete coordination europium at the origin of higher cohesive energy.<sup>43,47</sup> Indeed, a so high binding energy has already been observed in trivalent  $\text{EuPt}_5$  presenting divalent surface layer due to the surface valence transition.<sup>20</sup> In addition, in that case only one component is observed corresponding to the divalent surface state. Actually, the Eu 4f energy position is intrinsically linked to the cohesive energy and the work function of the bonded element. Unfortunately, as we have only one  $\text{Eu}^{2+}$  contribution in 4f spectrum, the screened core-hole model<sup>43</sup> is not applicable to determine the cohesive energy. However, in pure ionic crystal, the cohesive energy is given by the interionic Coulomb interaction. This kind of interaction is of so long range that a very small fraction of defects or interactions with surrounding atoms dramatically affect the cohesive energy. In our case,  $\text{Eu}^{2+}$  species are embedded in hydrated trivalent europium salt and act as a divalent europium ion in an incomplete coordination configuration. Two parameters then affect the cohesive energy, the presence of water molecule and of  $\text{Eu}^{2+}$  defect in the crystal. Indeed, crystal structure shows that in pure  $\text{EuCl}_3 \cdot 6 \text{H}_2\text{O}$  salt, the europium ion is directly linked to  $\text{H}_2\text{O}$  molecules<sup>49,50</sup> and recent study has shown that this interaction contribute to the broadening in optical transitions.<sup>6</sup> In summary, the single Eu 4f contribution we measure combined with its high binding energy is in good agreement

with a unique  $\text{Eu}^{2+}$  ground state. This is in agreement with a divalent europium ion in an incomplete coordination configuration homogeneously distributed throughout the crystal. From the resonant spectrum, in figure 6, we can figure out the peculiarities of the  $4d \rightarrow 4f$  transitions. By integrating, at constant binding energy, the resonant photoemission intensity centered to the two resonant states, we obtain the profiles presented in the top panel of figure 6 where they are compared to the spectral shape measured in Total Electron Yield. The resonant lines are composed of mainly one asymmetric component centered at 139 eV in photon energy corresponding to divalent europium and a second one composed of two asymmetric features at 143 and 152 eV ascribed to the trivalent europium species.

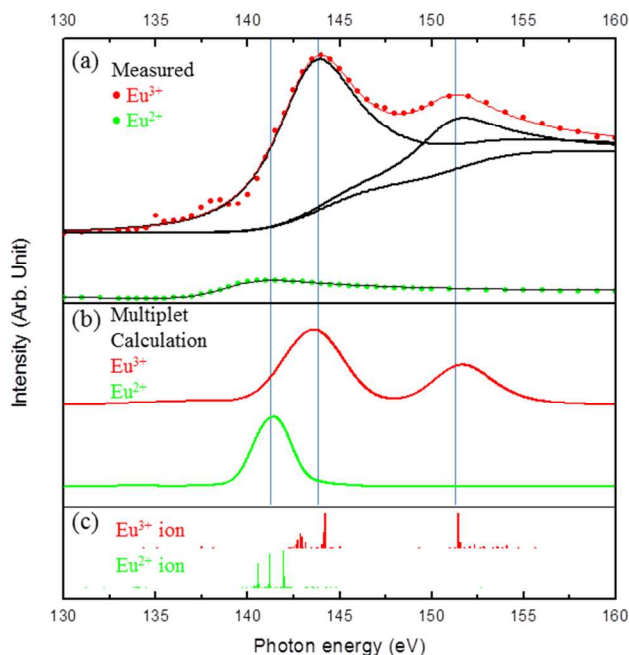


Fig. 6: (a)  $N_{4,5}$  absorption edges measured in partial electron yield integrating around the resonant lines located at 2 eV and 8.3 eV binding energy with Fano like profiles calculations. The Red curve is decomposed in the two asymmetric Fano profiles and a continuum steps lineshape background while the green curve is only composed of one asymmetric Fano profile. (b)  $\text{Eu}^{2+}$  and  $\text{Eu}^{3+}$  calculated XAS spectra at  $4d \rightarrow 4f$  absorption edge using the CTM4XAS 5.23 program (in green and red, respectively) The comparison of line profiles shows a proportion of 14.6% of  $\text{Eu}^{2+}$  and 85.3% of  $\text{Eu}^{3+}$  species (c) Representation of discrete energy states of intra-atomic multiplet excitation of  $\text{Eu}^{2+}$  and  $\text{Eu}^{3+}$  ions.

The partial yield lineshapes can be compared with those computed from atomic multiplet model reported in the central panel of Figure 6. In the bottom of figure 6c, we present the discrete energy states of intra-atomic multiplet  $4d \rightarrow 4f$  excitations of  $\text{Eu}^{2+}$  and  $\text{Eu}^{3+}$  ions. The broadening of discrete energy states leads to calculated XAS spectra figure 6c. Atomic multiplet calculations at the  $4d \rightarrow 4f$  transition are performed with a lifetime broadening of the core hole of 0.2 eV, calculated natural width of Eu 4d states<sup>42</sup> and an instrumental resolution broadening of 0.7 eV and 1.5 eV for divalent and trivalent europium, respectively, as found in the Eu 4d core level

spectra. We obtain a good agreement in terms of position and of balance between the different components corresponding to divalent and trivalent Europium species. However, this model doesn't describe the broadening and the asymmetric shape of the different components. The asymmetry of the  $4d \rightarrow 4f$  resonant photoemission feature can be fitted using a Fano profile.<sup>51</sup> In agreement with Fano model, the interference of a discrete autoionized state with a continuum results in a typical asymmetric peak in excitation spectra. Giant resonant asymmetric profile verifies the following expression:

$$I = I_0 \frac{(q+\epsilon)^2}{1+q^2} + I_b \quad (1)$$

$$\epsilon = \frac{E_{\text{phot}} - E_r}{\Gamma/2}$$

where  $E_{\text{phot}}$  is the incident photon energy,  $E_r$  the energy at resonance,  $I_0$  and  $I_b$  are the intensity contributions to transitions from continuum toward states that interact (i.e. resonant contribution) and do not interact (i.e. nonresonant part of the signal) with the discrete autoionized state, respectively.  $|q|$  is the Fano asymmetry parameter related to the lineshape and  $\Gamma$  indicates the spectral width of the autoionized state. In Figure 6, we present an asymmetric Fano profile for the divalent and trivalent Europium contributions.

$\text{Eu}^{2+}$  component matches well with a unique asymmetric component verifying equation (1).  $\text{Eu}^{3+}$  is a sum of two asymmetric components superimposed onto a continuum steps lineshape background.<sup>52</sup> We take a width of the steps equal to the linewidth of the  $\text{Eu}^{3+}$  resonant components. According to equation (1), the calculated energy resonances  $E_r$  at Eu  $4d \rightarrow 4f$  transition for  $\text{Eu}^{2+}$  and  $\text{Eu}^{3+}$  main components are equal to 139 eV for  $\text{Eu}^{2+}$  and 143 eV for the first component of  $\text{Eu}^{3+}$  species and 152 eV for the second one, respectively. The linewidth of the  $\text{Eu}^{2+}$  state is about 6.6 eV while the two components of the  $\text{Eu}^{3+}$  states present a lower natural linewidth of 5.5 eV. The linewidths of the autoionized state are somewhat broader compared with the theoretical energy states spread (tick figure) combined with the experimental enlargement determined in Eu 4d core level photoemission spectra (Fig 2). The asymmetric parameter  $|q|$  is lower in the case of  $\text{Eu}^{2+}$  ( $|q_{\text{Eu}^{2+}}|=1.5$ ) states compared to the  $\text{Eu}^{3+}$  states ( $|q_{\text{Eu}^{3+}}|=12.5$ ). This means that  $\text{Eu}^{2+}$  states exhibit stronger interactions between the discrete state and the states of the continuum.<sup>53</sup> These interactions are also visible in core level photoemission as discussed previously in Fig. 2 where  $\text{Eu}^{3+}$  core level components exhibit a standard Voigt doublet taking into accounts for the spin orbit splitting of the  $4d_{3/2}$  and  $4d_{5/2}$  states whereas  $\text{Eu}^{2+}$  contribution presents asymmetric shape due to d-hole and the ground state coupling. The results are in good agreement with Fano models,  $\text{Eu}^{2+}$  state can be understood as an interaction of one discrete state with states of a continuum while  $\text{Eu}^{3+}$  exhibits a behavior characteristic of the interaction of one discrete state with states of two or more continua.

Indeed, the interaction of one discrete state with states of two or more continua results in an asymmetric peak, as for the interaction between one state and one continuum, superposed on a smooth



background.<sup>51,54</sup> The origin of 4d→4f asymmetric shape resonance has been abundantly discussed for years.<sup>55-61</sup> However, since Eu is known to be a highly spin polarized system, new calculation based on the dynamic electron correlation decomposing in spin-up and spin-down states the contribution of 4d electrons have shown that a sharp resonance of 4d spin-up electrons (quasi-bound state) interaction with a broad resonance of 4d spin-down electrons (viewed as a continuum) is responsible for the 4d giant resonance exhibiting strong asymmetric Fano profile.<sup>62</sup> This explanation is also consistent with the multiplet structure observed for the 3d→4f transitions: while the 4d level exhibits a low spin orbit splitting of about 5 eV,<sup>63</sup> the spin-up and spin-down electrons are close enough to interact together so as to lead to giant resonance with Fano shape profile, the 3d levels presents higher spin orbit splitting beyond 30 eV<sup>63</sup> avoiding spin-up and spin-down electrons interactions and leading to resonance in good agreement with atomic multiplet calculations.

Removing the background from the different line profiles (fig. 6a), we integrate the area of each resonant line profile at 4d→4f transitions associated with the Eu<sup>3+</sup> and Eu<sup>2+</sup> species to determine their relative weight. The comparison of the two areas gives a percentage of 85% of Eu<sup>3+</sup> and 15% of Eu<sup>2+</sup> species for an inelastic electron mean free path of 5.72 Å. This result confirms the amounts found at 3d→4f transitions corresponding to a higher inelastic mean free path of 21.76 Å. We show that the amount of Eu<sup>2+</sup> species remains constant as a function of the sample depth. The Eu<sup>2+</sup> species are homogeneously distributed into the film.

The measurement of 4d→4f resonant photoemission spectra corroborates the results obtained at 3d→4f absorption edge. In both case we clearly identify signature of divalent and trivalent europium ions. In opposition to other works done on EuF<sub>3</sub> thin film presenting two different spectroscopic signatures at 3d→4f and 4d→4f transitions<sup>33</sup>, our sample doesn't exhibit any probed depth dependence. Eu<sup>2+</sup> and Eu<sup>3+</sup> electronic features relative weight measured at M<sub>4,5</sub> and N<sub>4,5</sub> absorption edges represent 15 and 85%, respectively, which correspond to a EuCl<sub>2,85</sub> mixed valence salt close to the EuCl<sub>2,85±0.05</sub> composition determined by chemical dosing. This result confirms a homogeneous surface and bulk repartition of the two Eu<sup>2+</sup> and Eu<sup>3+</sup> oxidation states in the sample with no surface-induced valence transition to the divalent state.<sup>18</sup>

## Conclusions

By measuring the Eu 4d core level spectra as a function of the photon energy, the spectral signature of Eu<sup>2+</sup> and Eu<sup>3+</sup> states of hydrated EuCl<sub>2,85</sub> salt has been evidenced. When compared to the trivalent europium, the divalent europium presents a complex feature due to 4d→4f interactions. Both contributions exhibit broad line shape. This feature is attributed to defects, due to the coexistence of divalent and trivalent ions in the crystal and to the interaction with surrounding water molecules. In particular, the spectroscopic signature of the divalent europium shows that the ion lies in an incomplete coordination configuration. The amount of the divalent and trivalent ions remains constant as a function of the sample depth. These results are in good agreement with a homogeneous distribution

of the divalent europium into the film. Core level photoemission spectroscopy is a very efficient and accurate technique to determine a spatial concentration profile by comparing the evolution in shape of the core level spectra by varying the probing depth. The calculated composition of the salt presents a slight deviation compared to the composition determined by the chemical analysis. The uncertainty originates from the difficulty to disentangle the signals coming from the Eu(II) and Eu(III) species deeply entangled and superimposed upon a complex background.

By comparison, a more precise quantification of the two species is obtained from resonant photoemission experiments in the valence band region performed at 3d→4f and 4d→4f absorption edges. We have shown that mixed-valence hydrated europium chloride thin film exhibits two well separated contributions corresponding to Eu<sup>2+</sup> and Eu<sup>3+</sup> spectroscopic signatures. The multiplet calculation, in good agreement with 3d→4f photoabsorption, allowed us to clearly identify the Eu<sup>2+</sup> and Eu<sup>3+</sup> contributions as measured in partial electron yield. The spectra obtained by integrating the resonant intensity located around 2 eV and 8 eV binding energies are well understood and identified by calculations and corresponding XAS Total electron yield spectral shapes. All the observed contributions can be assigned to Eu<sup>2+</sup> and Eu<sup>3+</sup> valence states, respectively.

Similarly, the resonant photoemission spectra at 4d→4f transition exhibits two main de-excitation pathways related to divalent and trivalent europium ions. At lower photon energy the giant resonance shape is obviously characteristic of Fano-like line shapes. This effect related to transitions from localized excited states to continuum is most pronounced for 4d→4f transition while it is not observable for 3d→4f absorption spectra which can be reproduced by atomic multiplet calculation, provided that the broadenings due to experimental resolution and core-hole lifetime of atomic multiplet discrete energy states are taken into account. The integration of Eu<sup>2+</sup> and Eu<sup>3+</sup> resonant states across the M<sub>4,5</sub> and N<sub>4,5</sub> absorption edges gives profile lines with relative weights close to 15 and 85% (respectively) at both edges. The relative weight in electronic behavior is in perfect agreement with the chemical composition of the salt.

From the combination of the core level photoemission spectra and resonant photoemission spectra, we have emphasized the robustness and accuracy in chemical depth profiling of ionic solids. Applied to hydrated mixed valence EuCl<sub>2,85</sub>, we have demonstrated the homogeneous distribution of the divalent europium in the crystal leading to a bulk n doping of the salt.

These spectroscopic techniques exhibit a very high sensitivity to chemical species down to 0.1 atomic percent.<sup>64</sup> They provide an efficient alternative to conventional chemical analysis to detect impurities at low concentration.

## Notes and references

<sup>a</sup> TEMPO Beamline, Synchrotron SOLEIL, St Aubin, BP 48, 91192 Gif-sur-Yvette cedex, France.

<sup>b</sup> Service de Physique de l'Etat Condensé, CEA-CNRS UMR 3680, Institut Rayonnement Matière de Saclay (IRAMIS), F-91191 Gif-sur-Yvette Cedex, France.

- <sup>c</sup> Institut Lumière Matière - UMR 5306 - Bât Jules Raulin ; 22, avenue Gaston Berger – Domaine de la Doua 69622 Villeurbanne Cedex, France.
- <sup>d</sup> Université Reims Champagne-Ardenne, ICMR UMR CNRS n°7312; Groupe Chimie de Coordination, BP 1039 - 51687 Reims Cedex 2, France.
- 1 L. M. Moreno, *Europium: Compounds, Production and Applications*, Nova Science Publishers, Inc., Hauppauge NY, 2011.
  - 2 H. de Riedmatten, M. Afzelius, M. U. Staudt, C. Simon and N. Gisin, *Nature*, 2008, **456**, 773-777.
  - 3 E. Fraval, M. J. Sellars and J. J. Longdell, *Physical Review Letters*, 2005, **95**, 030506.
  - 4 A. L. Alexander, J. J. Longdell, M. J. Sellars and N. B. Manson, *Physical Review Letters*, 2006, **96**, 043602.
  - 5 J. J. Longdell, E. Fraval, M. J. Sellars and N. B. Manson, *Physical Review Letters*, 2005, **95**, 063601.
  - 6 R. L. Ahlefeldt, A. Smith and M. J. Sellars, *Physical Review B*, 2009, **80**, 205106.
  - 7 J. C. G. Bunzli and C. Piguet, *Chemical Society Reviews*, 2005, **34**, 1048-1077.
  - 8 A. Matsko, D. Strelakov and L. Maleki, *Optics Express*, 2005, **13**, 2210-2223.
  - 9 M. Fleischhauer and M. Lukin, *Physical Review Letters*, 2000, **84**, 5094-5097.
  - 10 M. Fleischhauer, A. Imamoglu and J. Marangos, *Reviews of Modern Physics*, 2005, **77**, 633-673.
  - 11 W. Dehorrocks and M. Albin, *Progress in Inorganic Chemistry*, 1983, **31**, 1-104.
  - 12 M. G. Silly, S. Blanchandin, F. Sirotti, F. Lux, S. Chevreux, G. Lemerrier and F. Charra, *The Journal of Physical Chemistry C*, 2013, **117**, 9766-9771.
  - 13 S. Kasap, P. Capper and H. Tuller, in *Springer Handbook of Electronic and Photonic Materials*, Springer US, Editon edn., 2007, pp. 213-228.
  - 14 M. R. Oliver, J. O. Dimmock, A. L. McWhorter and T. B. Reed, *Physical Review B*, 1972, **5**, 1078-1098.
  - 15 A. Schmehl, V. Vaithyanathan, A. Herrnberger, S. Thiel, C. Richter, M. Liberati, T. Heeg, M. Rokerath, L. F. Kourkoutis, S. Muhlbauer, P. Boni, D. A. Muller, Y. Barash, J. Schubert, Y. Idzerda, J. Mannhart and D. G. Schlom, *Nature Materials*, 2007, **6**, 882-887.
  - 16 R. P. Panguluri, T. S. Santos, E. Negusse, J. Dvorak, Y. Idzerda, J. S. Moodera and B. Nadgorny, *Physical Review B*, 2008, **78**, 125307.
  - 17 S. G. Altendorf, A. Efimenko, V. Oliana, H. Kierspel, A. D. Rata and L. H. Tjeng, *Physical Review B*, 2011, **84**, 155442.
  - 18 G. K. Wertheim and G. Crececius, *Physical Review Letters*, 1978, **40**, 813-816.
  - 19 B. Johansson, *Physical Review B*, 1979, **19**, 6615-6619.
  - 20 E. J. Cho, S. J. Oh, S. Suga, T. Suzuki and T. Kasuya, *Journal of Electron Spectroscopy and Related Phenomena*, 1996, **77**, 173-181.
  - 21 E. J. Cho and S. J. Oh, *Physical Review B*, 1999, **59**, R15613-R15616.
  - 22 W. D. Schneider, C. Laubschat, I. Nowik and G. Kaindl, *Physical Review B*, 1981, **24**, 5422-5425.
  - 23 M. P. Seah and W. A. Dench, *Surf. Interface Anal.*, 1979, **1**, 2-11.
  - 24 C. D. Wagner, L. E. Davis and W. M. Riggs, *Surf. Interface Anal.*, 1980, **2**, 53-55.
  - 25 C. Laubschat, E. Weschke, G. Kalkowski and G. Kaindl, *Physica Scripta*, 1990, **41**, 124-129.
  - 26 C. Felser, J. Kohler, A. Simon, O. Jepsen, G. Svensson, S. Cramm and W. Eberhardt, *Physical Review B*, 1998, **57**, 1510-1514.
  - 27 K. Yamamoto, K. Horiba, M. Taguchi, M. Matsunami, N. Kamakura, A. Chainani, Y. Takata, K. Mimura, M. Shiga, H. Wada, Y. Senba, H. Ohashi and S. Shin, *Physical Review B*, 2005, **72**, 161101.
  - 28 S. Banik, A. Bendounan, A. Thamizhavel, A. Arya, P. Risterucci, F. Sirotti, A. K. Sinha, S. K. Dhar and S. K. Deb, *Physical Review B*, 2012, **86**, 085134.
  - 29 B. A. Orłowski, P. Dziawa, B. Kowalski, I. Kowalik, M. Pietrzyk, V. Osinniy, T. Story, S. Mickiewicz and R. Jonhson, *Applied Surface Science*, 2006, **252**, 5379-5383.
  - 30 B. A. Orłowski, B. J. Kowalski, M. Pietrzyk and R. Buczek, *Acta Physica Polonica A*, 2008, **114**, S103-S114.
  - 31 W. D. Schneider, C. Laubschat, G. Kalkowski, J. Haase and A. Puschmann, *Physical Review B*, 1983, **28**, 2017-2022.
  - 32 J. Szade, W. Burian, Z. Celinski, T. O'Keevan, M. Zangrando, F. Bondino and E. Magnano, *Surface Science*, 2005, **580**, 163-166.
  - 33 J. Szade, W. Burian, M. Zangrando, F. Bondino, E. Magnano, S. Widuch and Z. Celinski, *Surface Science*, 2008, **602**, 1525-1531.
  - 34 M. Zhuravleva, S. Friedrich and C. L. Melcher, *Optical Materials*, 2014, **36**, 670-674.
  - 35 F. Polack, M. Silly, C. Chauvet, B. Lagarde, N. Bergéard, M. Izquierdo, O. Chubar, D. Krizmancic, M. Ribbens, J. P. Duval, C. Basset, S. Kubsy and F. Sirotti, 10th International Conference on Synchrotron Radiation Instrumentation, Melbourne, AUSTRALIA. AIP Conf. Proc., 2010, **1234**, 185.
  - 36 N. Bergéard, M. G. Silly, D. Krizmancic, C. Chauvet, M. Guzzo, J. P. Ricaud, M. Izquierdo, L. Stebel, P. Pittana, R. Sergio, G. Cautero, G. Dufour, F. Rochet and F. Sirotti, *Journal of Synchrotron Radiation*, 2011, **18**, 245-250.
  - 37 E. Stavitski and F. M. F. de Groot, *Micron*, 2010, **41**, 687-694.
  - 38 R. Cowan, *The Theory of Atomic Structure and Spectra*, University of California Press, Berkeley, 1981.
  - 39 S. Tanuma, C. J. Powell and D. R. Penn, *Surf. Interface Anal.*, 1994, **21**, 165-176.
  - 40 P. D. L., *Handbook of Inorganic Compounds*, Second Edition edn., CRC Press, 2011.
  - 41 P. A. Bruhwiler, O. Karis and N. Martensson, *Reviews of Modern Physics*, 2002, **74**, 703-740.
  - 42 C. Gerth, K. Godehusen, M. Richter, P. Zimmermann, J. Schulz, P. Wernet, B. Sonntag, A. G. Kochur and I. D. Petrov, *Physical Review A*, 2000, **61**, 022713.
  - 43 B. Johansson and N. Martensson, *Physical Review B*, 1980, **21**, 4427-4457.
  - 44 C. Caspers, M. Muller, A. X. Gray, A. M. Kaiser, A. Gloskovskii, C. S. Fadley, W. Drube and C. M. Schneider, *Physica Status Solidi-Rapid Research Letters*, 2011, **5**, 441-443.
  - 45 B. T. Thole, G. Vanderlaan, J. C. Fuggle, G. A. Sawatzky, R. C. Karnatak and J. M. Esteva, *Physical Review B*, 1985, **32**, 5107-5118.
  - 46 J. B. Goedkoop, B. T. Thole, G. Vanderlaan, G. A. Sawatzky, F. M. F. Degroot and J. C. Fuggle, *Physical Review B*, 1988, **37**, 2086-2093.
  - 47 N. Martensson, B. Reihl, W. D. Schneider, V. Murgai, L. C. Gupta and R. D. Parks, *Physical Review B*, 1982, **25**, 1446-1448.

- 48 S. Iacobucci, F. Sirotti, M. Sacchi and G. Stefani, *Journal of Electron Spectroscopy and Related Phenomena*, 2002, **123**, 397-401.
- 49 D. L. Kepert, J. M. Patrick and A. H. White, *Australian Journal of Chemistry*, 1983, **36**, 477-482.
- 50 N. K. Belskii and Y. T. Struchkov, *Sov. Phys. Cryst.*, 1965, **10**, 15.
- 51 U. Fano, *Physical Review*, 1961, **124**, 1866.
- 52 J. Stöhr, *NEXAFS Spectroscopy*, XV edn., Springer, 1992.
- 53 R. Kumar, *Indian Journal of Physics*, 2013, **87**, 49-52.
- 54 U. Fano and J. W. Cooper, *Physical Review*, 1965, **137**, 1364.
- 55 J. W. Cooper, *Physical Review Letters*, 1964, **13**, 762.
- 56 K. T. Cheng and C. F. Fischer, *Physical Review A*, 1983, **28**, 2811-2819.
- 57 K. T. Cheng and W. R. Johnson, *Physical Review A*, 1983, **28**, 2820-2828.
- 58 U. Becker, H. G. Kerkhoff, D. W. Lindle, P. H. Kobrin, T. A. Ferrett, P. A. Heimann, C. M. Truesdale and D. A. Shirley, *Physical Review A*, 1986, **34**, 2858-2864.
- 59 M. Richter, M. Meyer, M. Pahler, T. Prescher, E. Vonraven, B. Sonntag and H. E. Wetzel, *Physical Review A*, 1989, **39**, 5666-5675.
- 60 M. Richter, M. Meyer, M. Pahler, T. Prescher, E. Vonraven, B. Sonntag and H. E. Wetzel, *Physical Review A*, 1989, **40**, 7007-7019.
- 61 C. Pan, S. L. Carter and H. P. Kelly, *Physical Review A*, 1991, **43**, 1290-1300.
- 62 X. M. Tong, D. Kato, T. Watanabe and S. Ohtani, *Journal of Physics B-Atomic Molecular and Optical Physics*, 2000, **33**, 717-725.
- 63 *X-RAY DATA BOOKLET*, Center for X-ray Optics and Advanced Light Source, Lawrence Berkeley National Laboratory, 2009.
- 64 K. KISS, *Problem Solving with Microbeam Analysis*, Elsevier, 1988, vol. 7, ch. 9, pp. 148-153.